



Impact of Mass-Gap on the Dispersion Interaction of Nanoparticles with Graphene out of Thermal Equilibrium

Galina L. Klimchitskaya ^{1,2,*} , Constantine C. Korikov³, Vladimir M. Mostepanenko ^{1,2,4}  and Oleg Yu. Tsybin ²

¹ Central Astronomical Observatory at Pulkovo of the Russian Academy of Sciences, 196140 Saint Petersburg, Russia

² Peter the Great Saint Petersburg Polytechnic University, 195251 Saint Petersburg, Russia

³ Huawei Noah's Ark Lab, Krylatskaya str. 17, Moscow 121614, Russia

⁴ Kazan Federal University, 420008 Kazan, Russia

* Correspondence: g.klimchitskaya@gmail.com

Abstract: We consider the nonequilibrium dispersion force acting on nanoparticles on the source side of gapped graphene sheet. Nanoparticles are kept at the environmental temperature, whereas the graphene sheet may be either cooler or hotter than the environment. Calculation of the dispersion force as a function of separation at different values of the mass-gap parameter is performed using the generalization of the fundamental Lifshitz theory to the out-of-thermal-equilibrium conditions. The response of gapped graphene to quantum and thermal fluctuations of the electromagnetic field is described by the polarization tensor in (2+1)-dimensional space-time in the framework of the Dirac model. The explicit expressions for the components of this tensor in the area of evanescent waves are presented. The nontrivial impact of the mass-gap parameter of graphene on the nonequilibrium dispersion force, as compared to the equilibrium one, is determined. It is shown that, unlike the case of a pristine graphene, the nonequilibrium force preserves an attractive character. The possibilities of using the obtained results in the design of micro- and nanodevices incorporating nanoparticles and graphene sheets for their functionality are discussed.

Keywords: dispersion force; thermal nonequilibrium; nanoparticles; Lifshitz theory; graphene; polarization tensor; nanodevices

Citation: Klimchitskaya, G.L.; Korikov, C.C.; Mostepanenko, V.M.; Tsybin, O.Y. Impact of Mass-Gap on the Dispersion Interaction of Nanoparticles with Graphene out of Thermal Equilibrium. *Appl. Sci.* **2023**, *13*, 7511. <https://doi.org/10.3390/app13137511>

Academic Editor: Petr Korusenko

Received: 26 May 2023

Accepted: 23 June 2023

Published: 25 June 2023

Publisher's Note: MDPI stays neutral with regard to jurisdictional claims in published maps and institutional affiliations.

Copyright: © 2023 by the authors. Submitted to *Appl. Sci.* for possible open access publication under the terms and conditions of the Creative Commons Attribution (CC BY) license (<https://creativecommons.org/licenses/by/4.0/>).

1. Introduction

Investigation of interaction between nanoparticles and material surfaces of different nature is of profound importance for physics and its applications in nanotechnology, including bioelectronics (see, e.g., the articles and reviews [1–17]). The microparticle-surface interaction includes several contributions, among which are mechanical contact forces, Born repulsion, and attractive dispersion forces [18,19]. At separations between a nanoparticle and a surface exceeding several nanometers, the dispersion forces, which are also called the van der Waals or Casimir-Polder forces, become dominant. They are determined by the quantum and thermal fluctuations of the electromagnetic field.

The entirely new material, which finds increasing use in nanotechnology, is graphene, i.e., the plane sheet of carbon atoms arranged in a hexagonal lattice [20–22]. The dispersion (Casimir-Polder) interaction of graphene with different atomic systems [23–36] and nanoparticles [37–42] has been the subject of much investigation. The obtained results are finding ever-widening application in bioelectronics [43–46].

The implementation of interaction between nanoparticles and graphene to new generation of nanodevices called for a development of theoretical methods which make it possible to calculate the dispersion force as a function of all relevant parameters. These methods have been developed in the framework of the Lifshitz theory [47–49], by expressing the dispersion force between an atom or a nanoparticle and a graphene

sheet via the atomic (nanoparticle) electric polarizability and the polarization tensor of graphene [23–36]. In so doing, the polarization tensor of graphene was found [50–53] on the basis of first principles of thermal quantum field theory in the framework of the Dirac model [20–22].

The Lifshitz theory of dispersion forces is formulated for the case when the interacting bodies are in the state of thermal equilibrium with the environment. This condition, however, is violated when both of the interacting bodies (or at least one of them) are kept at temperatures different from that of the environment. The formalism generalizing the Lifshitz theory for systems out of thermal equilibrium was developed in [54–59]. During the last few years, different aspects of the nonequilibrium dispersion forces acting between two material plates, a small sphere or an atom and a material plate and between two spheres were investigated using this formalism [60–66]. Specifically, the case of temperature-dependent response functions of the interacting bodies was considered in [63,64].

The nonequilibrium dispersion force acting on spherical nanoparticles on the source side of an ideal (pristine) freestanding in vacuum graphene sheet was investigated quite recently [67]. The pristine character of graphene assumed in [67] means that its crystal lattice does not include any foreign atoms and the quasiparticles are massless, as was supposed in the original Dirac model [20–22]. Reference [67] suggested that the temperature of nanoparticles is the same as of the environment, whereas the graphene sheet can be either cooler or hotter than the environment. It was shown that an impact of the nonequilibrium effects of the dispersion force decreases with increasing graphene-nanoparticle separation distance. What is more, according to the results obtained, at relatively short separations the effects of nonequilibrium may change the sign of the dispersion force by making it repulsive [67].

In this article, we apply the theory of nonequilibrium dispersion interaction to investigate the force acting on nanoparticles kept at the environmental temperature on the source side of gapped graphene described by the Dirac model with light but massive quasiparticles. The temperature of a graphene sheet is assumed to be either lower or higher than that of the environment. To perform computations of the dispersion force in this case, we present the explicit expressions for the polarization tensor of gapped graphene along the real frequency axis in the region of evanescent waves, which have not been considered in the literature up to now with sufficient detail. We demonstrated that the value of the mass-gap parameter makes a nontrivial impact on the nonequilibrium force, as compared to the equilibrium one, depending on the values of separation and graphene temperature. Unlike the case of a pristine graphene, for a nonzero mass of quasiparticles the nonequilibrium dispersion force preserves its attractive character.

The structure of the article is as follows. In Section 2, we present the expression for a nonequilibrium dispersion force acting on nanoparticles on the source side of gapped graphene sheet in terms of the polarization tensor. In Section 3, the components of this tensor in the area of the evanescent waves are specified. Section 4 contains the computational results for the dispersion force acting on nanoparticles which is shown as the function of separation for different values of the mass-gap parameter and at different temperatures. In Sections 5 and 6, the reader will find the discussion of the obtained results and our conclusions.

2. Nonequilibrium Dispersion Force on a Nanoparticle on the Source Side of Gapped Graphene

We consider the dispersion (Casimir-Polder) force acting on a spherical nanoparticle of radius R spaced above a graphene sheet at a separation $a \gg R$. The consideration of nanoparticles of other types (for instance, having a nonspherical shape) would need a more complicated theory using the scattering-matrix approach [58]. The area of graphene sheet is taken to be much larger than the separation to a nanoparticle squared. It is assumed that at all temperatures T under consideration it holds $R \ll \hbar c / (k_B T)$, where k_B is the Boltzmann constant [for instance, at the environmental temperature

$T_E = 300$ K one has $\hbar c / (k_B T) \approx 7.6 \mu\text{m}$]. Under this condition, within the range of separations a considered below, the nanoparticle can be described by the static polarizability $\alpha(0)$, which takes the form [61]

$$\alpha(0) = R^3 \frac{\varepsilon(0) - 1}{\varepsilon(0) + 1}, \quad \alpha(0) = R^3 \quad (1)$$

for dielectric and metallic nanoparticles, respectively, where $\varepsilon(0)$ is the static dielectric permittivity of a nanoparticle material.

Below we assume that nanoparticles have the same temperature T_E as the environment, whereas the graphene sheet has the temperature T_g which is either lower or higher than T_E . As distinct from [67], where the case of a pristine graphene was considered, here the graphene sheet is characterized by a nonzero mass-gap parameter $\Delta = 2mv_F^2$, where m is the mass of quasiparticles and $v_F \approx c/300$ is the Fermi velocity [21,68,69].

The nonequilibrium dispersion force, acting on a nanoparticle, is represented in the form [56,58]

$$F_{\text{neq}}(a, \Delta, T_E, T_g) = F_M(a, \Delta, T_E, T_g) + F_r(a, \Delta, T_E, T_g), \quad (2)$$

where $F_M(a, \Delta, T_E, T_g)$ can be expressed as a sum over the discrete Matsubara frequencies, much as the equilibrium Casimir-Polder force [70,71], whereas $F_r(a, \Delta, T_E, T_g)$ is the contribution which is given by an integral over the real frequency axis.

In fact, the effects of nonequilibrium contribute to both terms in the right-hand side of (2). Because of this, it is not reasonable to call the first of them "equilibrium" and the second — "nonequilibrium" that occurs in the literature. Moreover, the division of F_{neq} into F_M and F_r is not unique and can be made in a number of ways. Below we use the same division as in [67].

In this case, the first term in (2) is given by [67]

$$F_M(a, \Delta, T_E, T_g) = -\frac{2k_B T_E \alpha(0)}{c^2} \sum_{l=0}^{\infty} \int_0^{\infty} k dk e^{-2aq_l(k)} \times \left\{ \left[2q_l^2(k)c^2 - \xi_{E,l}^2 \right] R_{\text{TM}}(i\xi_{E,l}, k; \Delta, T_g) - \xi_{E,l}^2 R_{\text{TE}}(i\xi_{E,l}, k; \Delta, T_g) \right\}. \quad (3)$$

Here, k is the magnitude of the wave vector component along the graphene sheet, $q_l^2(k) = k^2 + \xi_{E,l}^2/c^2$, $\xi_{E,l} = 2\pi k_B T_E l / \hbar$ with $l = 0, 1, 2, \dots$ are the Matsubara frequencies at the environmental temperature T_E , and the prime on the summation sign multiplies the term with $l = 0$ by the factor $1/2$.

The quantities R_{TM} and R_{TE} are the reflection coefficients of the electromagnetic fluctuations on a graphene sheet for the transverse magnetic (TM) and transverse electric (TE) polarizations calculated at the pure imaginary Matsubara frequencies $\omega = i\xi_{E,l}$, but at the temperature of graphene T_g . They are expressed via the components of the polarization tensor of graphene $\Pi_{ij}(\omega, k; \Delta, T_g)$ [51,52,72]

$$R_{\text{TM}}(\omega, k; \Delta, T_g) = \frac{q(\omega, k) \Pi_{00}(\omega, k; \Delta, T_g)}{2\hbar k^2 + q(\omega, k) \Pi_{00}(\omega, k; \Delta, T_g)},$$

$$R_{\text{TE}}(\omega, k; \Delta, T_g) = -\frac{\Pi(\omega, k; \Delta, T_g)}{2\hbar k^2 q(\omega, k) + \Pi(\omega, k; \Delta, T_g)}, \quad (4)$$

where $q^2(\omega, k) = k^2 - \omega^2/c^2$ and the quantity Π is defined as

$$\Pi(\omega, k; \Delta, T_g) = k^2 \Pi_i^i(\omega, k; \Delta, T_g) - q^2(\omega, k) \Pi_{00}(\omega, k; \Delta, T_g) \quad (5)$$

with the summation over the repeated index $i = 0, 1, 2$. The explicit expressions for the polarization tensor in the required frequency regions are given in the next section.

Note that the polarization tensor Π_{ij} describing the response of graphene to quantum and thermal fluctuations of the electromagnetic field strongly depends on temperature T_g as a parameter. In application to the nonequilibrium dispersion forces, similar situation was considered previously for the phase-change [63] and metallic [64] materials.

The second term on the right-hand side of (2), according to the division accepted in [67], takes the form [58]

$$F_r(a, \Delta, T_E, T_g) = \frac{2\hbar\alpha(0)}{\pi c^2} \int_0^\infty d\omega \Theta(\omega, T_E, T_g) \int_{\omega/c}^\infty k dk e^{-2aq(\omega, k)} \times \text{Im} \left\{ \left[2q^2(\omega, k)c^2 + \omega^2 \right] R_{\text{TM}}(\omega, k; \Delta, T_g) + \omega^2 R_{\text{TE}}(\omega, k; \Delta, T_g) \right\}. \quad (6)$$

Here, the quantity $\Theta(\omega, T_E, T_g)$ is defined as

$$\Theta(\omega, T_E, T_g) = \frac{1}{\exp\left(\frac{\hbar\omega}{k_B T_E}\right) - 1} - \frac{1}{\exp\left(\frac{\hbar\omega}{k_B T_g}\right) - 1}. \quad (7)$$

The important property of the division (2) accepted in [67] is that the quantity F_r expressed in terms of real frequencies is determined by the contribution of only the evanescent waves for which $k > \omega/c$. As a result, the exponent in (6) has the real power. This is advantageous as compared to the standard Lifshitz formula for equilibrium Casimir and Casimir-Polder forces written in terms of real frequencies, which contains the contributions of both the evanescent and propagating ($k < \omega/c$) waves [71]. For the latter contribution, the quantity $q(\omega, k)$ is pure imaginary resulting in the integral of quickly oscillating function which makes integration difficult.

3. Polarization Tensor in the Area of Evanescent Waves

The nonequilibrium dispersion force (2) acting on nanoparticles on the source of a gapped graphene sheet can be computed by Equations (3)–(7). For this purpose, one should know the component of the polarization tensor Π_{00} and the combination of its components Π defined in (5) for a graphene sheet with the nonzero mass-gap parameter Δ . As mentioned in Section 1, the polarization tensor of graphene was found in [50–53] in the framework of the Dirac model. In doing so, [50] was devoted to the case of zero temperature, $T = 0$. In [51] the polarization tensor of graphene was obtained at nonzero temperature at all discrete Matsubara frequencies. These results, however, did not admit a continuation to the entire plane of complex frequencies and, specifically, were inapplicable along the real frequency axis. Thus, they can be used for calculation of the equilibrium Casimir and Casimir-Polder forces and the contribution F_M to the nonequilibrium force, but not the contribution F_r .

The polarization tensor of graphene with nonzero Δ valid over the entire plane of complex frequencies was derived in [52], where the most attention was paid to the region of propagating waves $k < \omega/c$ in connection with the topical applications to the reflectivity [73–76] and conductivity [77–80] properties of graphene. Below we present a more detailed exposition of the results of [52] relevant to the area of evanescent waves ($k > \omega/c$) which determine the contribution (6) to the nonequilibrium dispersion force.

Before dealing with the polarization tensor, a few remarks concerning the area of application of this quantity for the calculation of dispersion forces are in order. In [50–53], the polarization tensor of graphene was derived in the framework of the Dirac model. This model provides the physically adequate description of graphene at energies below approximately 3 eV [81]. Thus, the energies $\hbar\omega$ giving the major contribution

to the dispersion force should be below this limit. The characteristic frequency determining the dispersion force is $\omega_c = c/(2a)$ [70,71]. It is easily seen that the respective characteristic energy $\hbar\omega_c$ is below 1 eV at all separations $a > 100$ nm. Therefore, at separations, say, $a > 200$ nm one can safely use the Dirac model and its consequences in calculations of dispersion forces. This was confirmed by the fact that measurements of the dispersion interaction with graphene were found in a very good agreement with theoretical predictions computed using the polarization tensor [82,83].

Now we present the explicit expressions for the quantities Π_{00} and Π in the frequency region of evanescent waves $\omega/c < k$. Similar to [30], we present these quantities as the sums of two contributions

$$\begin{aligned}\Pi_{00}(\omega, k; \Delta, T_g) &= \Pi_{00}^{(0)}(\omega, k; \Delta) + \Pi_{00}^{(1)}(\omega, k; \Delta, T_g), \\ \Pi(\omega, k; \Delta, T_g) &= \Pi^{(0)}(\omega, k; \Delta) + \Pi^{(1)}(\omega, k; \Delta, T_g).\end{aligned}\quad (8)$$

Here, the contributions with an upper index (0) are defined at zero temperature, $T = 0$, whereas the quantities with an upper index (1) have a meaning of the thermal corrections to them. In doing so, both contributions depend on the mass-gap parameter of graphene Δ . With vanishing temperature, both $\Pi_{00}^{(1)}$ and $\Pi^{(1)}$ go to zero.

The analytic continuation of the polarization tensor of graphene to the frequency region of evanescent waves takes different forms in the interval

$$\frac{\omega}{c} < k \leq \frac{\omega}{v_F} \approx 300 \frac{\omega}{c} \quad (9)$$

and in the interval

$$300 \frac{\omega}{c} \approx \frac{\omega}{v_F} < k < \infty. \quad (10)$$

First, we consider the interval (9) which is often called the plasmonic region [84]. In this region the first contributions to (8) take the form [52]

$$\begin{aligned}\Pi_{00}^{(0)}(\omega, k; \Delta) &= -\frac{2\alpha k^2}{cp^2(\omega, k)} \Phi(\omega, k, \Delta), \\ \Pi^{(0)}(\omega, k; \Delta) &= \frac{2\alpha k^2}{c} \Phi(\omega, k, \Delta),\end{aligned}\quad (11)$$

where

$$p^2(\omega, k) = \frac{\omega^2}{c^2} - \frac{v_F^2}{c^2} k^2 \geq 0 \quad (12)$$

and $\alpha = e^2/(\hbar c)$ is the fine structure constant. The function Φ is defined as

$$\Phi(\omega, k, \Delta) = \Delta - \hbar cp(\omega, k) \left[1 + \frac{\Delta^2}{\hbar^2 c^2 p^2(\omega, k)} \right] \left[\operatorname{arctanh} \frac{\Delta}{\hbar cp(\omega, k)} + i \frac{\pi}{2} \right] \quad (13)$$

for $\hbar cp(\omega, k) \geq \Delta$ and as

$$\Phi(\omega, k, \Delta) = \Delta - \hbar cp(\omega, k) \left[1 + \frac{\Delta^2}{\hbar^2 c^2 p^2(\omega, k)} \right] \operatorname{arctanh} \frac{\hbar cp(\omega, k)}{\Delta} \quad (14)$$

for $\hbar cp(\omega, k) < \Delta$.

The second contributions to (8) in the plasmonic region are more complicated. It is convenient to define their real and imaginary parts separately. We start from defining

the real parts of $\Pi_{00}^{(1)}$ and $\Pi^{(1)}$ which, in turn, have different forms under the conditions $\hbar cp(\omega, k) \geq \Delta$ and $\hbar cp(\omega, k) < \Delta$.

Thus, if the condition $\hbar cp(\omega, k) \geq \Delta$ is satisfied, one obtains from [52] after identical transformations

$$\operatorname{Re} \Pi_{00}^{(1)}(\omega, k; \Delta, T_g) = \frac{8\alpha\hbar c^2}{v_F^2}(I_1 + I_2 + I_3), \quad (15)$$

where the following notations are introduced:

$$\begin{aligned} I_1 &= \int_{\frac{\Delta}{2\hbar c}}^{u^{(-)}(\omega, k)} \frac{du}{e^{\beta(T_g)u} + 1} \left[2 - \frac{B_1(2cu + \omega) + B_1(2cu - \omega)}{cp(\omega, k)} \right], \\ I_2 &= \int_{u^{(-)}(\omega, k)}^{u^{(+)}(\omega, k)} \frac{du}{e^{\beta(T_g)u} + 1} \left[2 - \frac{B_1(2cu + \omega)}{cp(\omega, k)} \right], \\ I_3 &= \int_{u^{(+)}(\omega, k)}^{\infty} \frac{du}{e^{\beta(T_g)u} + 1} \left[2 - \frac{B_1(2cu + \omega) - B_1(2cu - \omega)}{cp(\omega, k)} \right]. \end{aligned} \quad (16)$$

Here,

$$\begin{aligned} u^{(\pm)}(\omega, k) &= \frac{1}{2c}[\omega \pm v_F k \sqrt{A(\omega, k; \Delta)}], \quad A(\omega, k; \Delta) = 1 - \frac{\Delta^2}{\hbar^2 c^2 p^2(\omega, k)}, \\ B_1(x) &= \frac{x^2 - v_F^2 k^2}{\sqrt{x^2 - v_F^2 k^2 A(\omega, k; \Delta)}}, \quad \beta(T_g) = \frac{\hbar c}{k_B T_g}. \end{aligned} \quad (17)$$

It is seen that all the integrals I_j are the functions of ω , k , Δ , and T_g .

Under the same condition $\hbar cp(\omega, k) \geq \Delta$, we obtain from [52]

$$\operatorname{Re} \Pi^{(1)}(\omega, k; \Delta, T_g) = \frac{8\alpha\hbar\omega^2}{v_F^2}(J_1 + J_2 + J_3), \quad (18)$$

where the quantities J_j are given by

$$\begin{aligned} J_1 &= \int_{\frac{\Delta}{2\hbar c}}^{u^{(-)}(\omega, k)} \frac{du}{e^{\beta(T_g)u} + 1} \left\{ 2 - \frac{cp(\omega, k)[B_2(2cu + \omega) + B_2(2cu - \omega)]}{\omega^2} \right\}, \\ J_2 &= \int_{u^{(-)}(\omega, k)}^{u^{(+)}(\omega, k)} \frac{du}{e^{\beta(T_g)u} + 1} \left[2 - \frac{cp(\omega, k)B_2(2cu + \omega)}{\omega^2} \right], \\ J_3 &= \int_{u^{(+)}(\omega, k)}^{\infty} \frac{du}{e^{\beta(T_g)u} + 1} \left\{ 2 - \frac{cp(\omega, k)[B_2(2cu + \omega) - B_2(2cu - \omega)]}{\omega^2} \right\}. \end{aligned} \quad (19)$$

Here, the function $B_2(x)$ is defined as

$$B_2(x) = \frac{x^2 - v_F^2 k^2 [1 - A(\omega, k; \Delta)]}{\sqrt{x^2 - v_F^2 k^2 A(\omega, k; \Delta)}}. \quad (20)$$

If the opposite condition, $\hbar cp(\omega, k) < \Delta$, is satisfied, the real parts of $\Pi_{00}^{(1)}$ and $\Pi^{(1)}$ take the form following from [52]

$$\begin{aligned} \operatorname{Re} \Pi_{00}^{(1)}(\omega, k; \Delta, T_g) &= \frac{8\alpha\hbar c^2}{v_F^2} \int_{\frac{\Delta}{2\hbar c}}^{\infty} \frac{du}{e^{\beta(T_g)u} + 1} \\ &\times \left[2 - \frac{B_1(2cu + \omega) - B_1(2cu - \omega)}{cp(\omega, k)} \right], \end{aligned} \quad (21)$$

$$\begin{aligned} \operatorname{Re} \Pi^{(1)}(\omega, k; \Delta, T_g) &= \frac{8\alpha\hbar\omega^2}{v_F^2} \int_{\frac{\Delta}{2\hbar c}}^{\infty} \frac{du}{e^{\beta(T_g)u} + 1} \\ &\times \left\{ 2 - \frac{cp(\omega, k)[B_2(2cu + \omega) - B_2(2cu - \omega)]}{\omega^2} \right\}. \end{aligned}$$

This concludes consideration of the real parts of $\Pi_{00}^{(1)}$ and $\Pi^{(1)}$ in the plasmonic region (9). As to the imaginary parts of $\Pi_{00}^{(1)}$ and $\Pi^{(1)}$, they are given by the unified expressions

$$\begin{aligned} \operatorname{Im} \Pi_{00}^{(1)}(\omega, k; \Delta, T_g) &= \frac{8\alpha\hbar c}{v_F^2 p(\omega, k)} \theta[\hbar cp(\omega, k) - \Delta] \\ &\times \int_{u^{(-)}(\omega, k)}^{u^{(+)}(\omega, k)} \frac{du}{e^{\beta(T_g)u} + 1} \frac{(2cu - \omega)^2 - v_F^2 k^2}{\sqrt{v_F^2 k^2 A(\omega, k; \Delta) - (2cu - \omega)^2}}, \end{aligned} \quad (22)$$

$$\begin{aligned} \operatorname{Im} \Pi^{(1)}(\omega, k; \Delta, T_g) &= \frac{8\alpha\hbar cp(\omega, k)}{v_F^2} \theta[\hbar cp(\omega, k) - \Delta] \\ &\times \int_{u^{(-)}(\omega, k)}^{u^{(+)}(\omega, k)} \frac{du}{e^{\beta(T_g)u} + 1} \frac{(2cu - \omega)^2 + v_F^2 k^2 [1 - A(\omega, k; \Delta)]}{\sqrt{v_F^2 k^2 A(\omega, k; \Delta) - (2cu - \omega)^2}}, \end{aligned}$$

which are valid over the entire region (9). Here, $\theta(x)$ is the step function equal to 1 for $x \geq 0$ and to 0 for $x < 0$.

Next, we consider the polarization tensor in the interval (10). In this case, the first contributions to (8) are given by [52]

$$\begin{aligned} \Pi_{00}^{(0)}(\omega, k; \Delta) &= \frac{\alpha\hbar k^2}{\tilde{p}(\omega, k)} \Psi(\omega, k, \Delta), \\ \Pi^{(0)}(\omega, k; \Delta) &= \alpha\hbar k^2 \tilde{p}(\omega, k) \Psi(\omega, k, \Delta), \end{aligned} \quad (23)$$

where

$$\tilde{p}^2(\omega, k) = \frac{v_F^2}{c^2} k^2 - \frac{\omega^2}{c^2} \geq 0 \quad (24)$$

and Ψ is defined as

$$\Psi(\omega, k, \Delta) = 2 \left\{ \frac{\Delta}{\hbar c \tilde{p}(\omega, k)} + \left[1 - \frac{\Delta^2}{\hbar^2 c^2 \tilde{p}^2(\omega, k)} \right] \arctan \frac{\hbar c \tilde{p}(\omega, k)}{\Delta} \right\}. \quad (25)$$

Similar to the plasmonic interval (9), in the interval (10) the quantities $\Pi_{00}^{(1)}$ and $\Pi^{(1)}$ are the complex-valued functions. Here, we present their explicit expressions do not separating the real and imaginary parts [52]

$$\begin{aligned}\Pi_{00}^{(1)}(\omega, k; \Delta, T_g) &= \frac{8\alpha\hbar c^2 \tilde{p}(\omega, k)}{v_F^2} \int_{\frac{\Delta}{\hbar c \tilde{p}(\omega, k)}}^{\infty} \frac{dv}{e^{D(\omega, k, T_g)v} + 1} \\ &\times \left[1 - \frac{1}{2} \sum_{\lambda=\pm 1} \frac{1 - v^2 - 2\lambda \frac{\omega}{c \tilde{p}(\omega, k)} v}{\sqrt{1 - v^2 - 2\lambda \frac{\omega}{c \tilde{p}(\omega, k)} v + \frac{v_F^2 k^2 \Delta^2}{c^4 \hbar^2 \tilde{p}^4(\omega, k)}}} \right], \\ \Pi^{(1)}(\omega, k; \Delta, T_g) &= \frac{8\alpha\hbar c^2 \tilde{p}(\omega, k)}{v_F^2} \int_{\frac{\Delta}{\hbar c \tilde{p}(\omega, k)}}^{\infty} \frac{dv}{e^{D(\omega, k, T_g)v} + 1} \\ &\times \left\{ \frac{\omega^2}{c^2} - \frac{1}{2} \sum_{\lambda=\pm 1} \frac{[\tilde{p}(\omega, k)v + \lambda \frac{\omega}{c}]^2 + \frac{v_F^2 k^2 \Delta^2}{c^4 \hbar^2 \tilde{p}^2(\omega, k)}}{\sqrt{1 - v^2 - 2\lambda \frac{\omega}{c \tilde{p}(\omega, k)} v + \frac{v_F^2 k^2 \Delta^2}{c^4 \hbar^2 \tilde{p}^4(\omega, k)}}} \right\},\end{aligned}\quad (26)$$

where

$$D(\omega, k, T_g) = \frac{\hbar c \tilde{p}(\omega, k)}{2k_B T_g}. \quad (27)$$

For calculation of the contribution F_M to the nonequilibrium dispersion force (2), which is given by (3), one also needs the values of the polarization tensor at the pure imaginary Matsubara frequencies. They are easily obtained from (8) and the respective expressions (23)–(27) found in the interval (10) where we put $\omega = i\zeta_{E,l}$. In this case the definitions (24) and (27) take the form

$$\tilde{p}^2(i\zeta_{E,l}, k) \equiv \tilde{p}_l^2(k) = \frac{v_F^2}{c^2} k^2 + \frac{\zeta_{E,l}^2}{c^2}, \quad D(i\zeta_{E,l}, k, T_g) = \frac{\hbar c \tilde{p}_l(k)}{2k_B T_g}. \quad (28)$$

Thus, all expressions for the polarization tensor appearing in both contributions F_M and F_r to the nonequilibrium dispersion force through the reflection coefficients (4) are presented.

4. Computational Results for the Dispersion Force on Nanoparticles from Graphene

Here, we present the computational results for the nonequilibrium dispersion force F_{neq} acting on nanoparticles of radius R on the source side of a graphene sheet characterized by the mass-gap parameter Δ which takes the typical values of 0.1 and 0.2 eV [82,83]. The temperature of nanoparticles is assumed to be the same as of the environment, i.e., $T_E = 300$ K, whereas the temperature of a graphene sheet can be either cooler, $T_g = 77$ K, or hotter, $T_g = 500$ K, than the environmental temperature. These temperatures are chosen as a representative example. The first of them is the temperature of liquid nitrogen, whereas the second is close to that employed in the experiment on measuring the nonequilibrium Casimir-Polder force [85]. The developed formalism allows computation of the nonequilibrium dispersion interaction for any experimental temperatures. In line with the assumptions made in Sections 2 and 3, computations are performed in the separation range from 200 nm to 2 μ m and it is assumed that R is sufficiently small. The polarizabilities of dielectric and metallic nanoparticles are presented in (1).

Numerical computations were performed by Equations (2)–(4) and (6), (7) using the expressions for the polarization tensor presented in Section 3. For this purpose, we worked out a program written in the C++ programming language. The program utilizes the Gauss-Kronrod and Double-exponential quadrature methods from the GNU Scientific Library [86] and Boost C++ Libraries [87] for numerical integration. High precision computation is achieved with the help of the Boost Multiprecision Library [88]. The program also employs the OpenMP Library [89] for parallelization. The results presented below were obtained using computational resources of the Supercomputer Center of the Peter the Great Saint Petersburg Polytechnic University.

The computational results for F_{neq} are normalized to the classical limit of the equilibrium dispersion force acting on a nanoparticle on the source side of an ideal metal plane [71]

$$F_c(a, T_E) = -\frac{3k_B T}{4a^4} \alpha(0). \quad (29)$$

The normalized values do not depend on the static polarizability of a nanoparticle $\alpha(0)$. The absolute values of F_{neq} for the nanoparticles made of some specific material can be obtained using Equations (1) and (29) by fixing the values of R and $\varepsilon(0)$. In doing so the value of R is restricted by only the conditions $R \ll a$ and $R \ll \hbar/(k_B T)$ considered in the beginning of Section 2.

In Figure 1, the ratio the F_{neq}/F_c is shown as a function of the nanoparticle-graphene separation by the two bottom (blue) lines plotted for graphene sheets with the mass-gap parameter Δ equal to 0.2 and 0.1 eV kept at temperature $T_g = 77$ K.

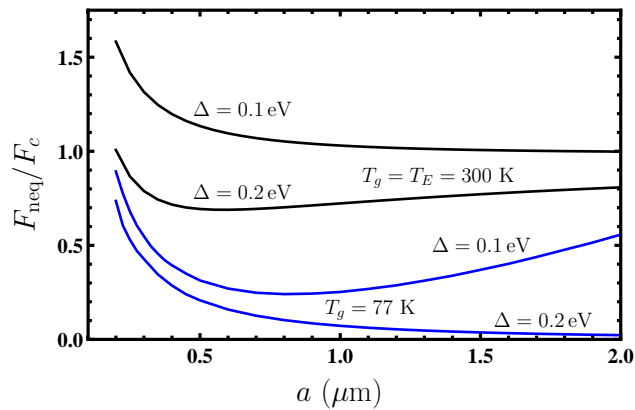


Figure 1. The ratio of nonequilibrium force acting on a nanoparticle on the source side of cooled to $T_g = 77$ K gapped graphene sheets with $\Delta = 0.2$ and 0.1 eV to the classical limit of an equilibrium at $T_E = 300$ K force acting between the same nanoparticle and an ideal metal plane is shown by the two blue bottom lines as the function of separation. The two black top lines show the ratio of the equilibrium force between a nanoparticle and the gapped graphene sheets kept at $T_E = 300$ K to the same classical limit.

For comparison purposes, the two top (black) lines in Figure 1 show the ratio F_{eq}/F_c for the same nanoparticles and graphene sheets computed in the state of thermal equilibrium, i.e., when the temperatures of graphene and nanoparticles are equal to the environmental temperature, $T_g = T_E = 300$ K. In this case, the quantity F_{eq} is computed as

$$F_{\text{eq}}(a, \Delta, T_E) = -\frac{2k_B T_E \alpha(0)}{c} \sum_{l=0}^{\infty} \int_0^{\infty} k dk e^{-2aq_l(k)} \times \left\{ \left[2q_l^2(k)c^2 - \zeta_{E,l}^2 \right] R_{\text{TM}}(i\zeta_{E,l}, k; \Delta, T_E) - \zeta_{E,l}^2 R_{\text{TE}}(i\zeta_{E,l}, k; \Delta, T_E) \right\}. \quad (30)$$

Equation (30) is obtained from (3) by putting $T_g = T_E$.

As is seen in Figure 1, for a cooled graphene sheet the change in the value of Δ makes a lesser impact on F_{neq} than on F_{eq} at short separations but, on the contrary, makes a greater impact on F_{neq} than on F_{eq} at large separations. As opposed to the case of cooled sheet of a pristine graphene [67], for a gapped graphene with sufficiently large Δ the nonequilibrium dispersion force remains attractive.

Now let us admit that the graphene sheet is heated up to $T_g = 500$ K, whereas nanoparticles preserve the environmental temperature $T_E = 300$ K. In this case, the computational results for the ratio F_{neq}/F_c are shown in Figure 2 as the functions of separation by the two red lines plotted for graphene sheets with the mass-gap parameter Δ equal to 0.2 and 0.1 eV. The two black lines, which show the ratio F_{eq}/F_c , are reproduced from Figure 1. As explained above, they are plotted for graphene sheets with $\Delta = 0.2$ and 0.1 eV in thermal equilibrium with the environment at $T_g = T_E = 300$ K.

From Figure 2, it is seen that for a heated graphene sheet the change in the value of Δ makes a lesser impact on F_{neq} than on F_{eq} over the entire separation region considered. By comparing Figures 1 and 2, one can conclude that the magnitude of a nonequilibrium dispersion force acting on a nanoparticle on the source side of gapped graphene increases with increasing temperature.

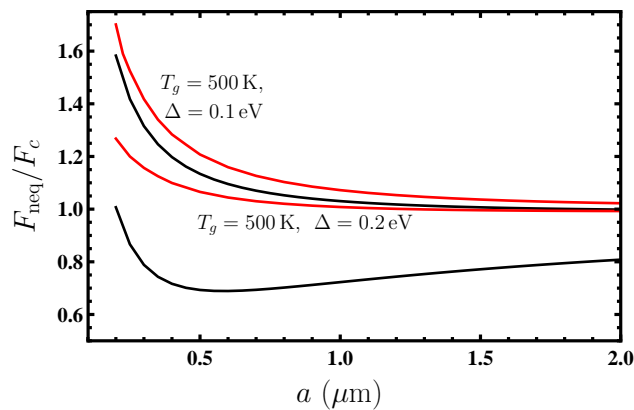


Figure 2. The ratio of nonequilibrium force acting on a nanoparticle on the source side of heated to $T_g = 500$ K gapped graphene sheets with $\Delta = 0.2$ and 0.1 eV to the classical limit of an equilibrium at $T_E = 300$ K force acting between the same nanoparticle and an ideal metal plane is shown by the two red lines as the functions of separation. The two black lines reproduced from Figure 1 show the ratio of the equilibrium force between a nanoparticle and the gapped graphene sheets kept at $T_E = 300$ K to the same classical limit.

Now we investigate the relative role of the first and second contributions F_M and F_r in (2), which sum represents the total value of F_{neq} . We begin with F_M computed by Equations (3) and (4) and respective expressions (8), (23)–(27) for the polarization tensor calculated at the pure imaginary Matsubara frequencies $i\zeta_{E,l}$. Similar to the case of an equilibrium force, F_M is always negative, i.e., contributes to the attraction. The computational results for the ratio F_M/F_c are shown as the functions of separation in Figure 3 by the two pairs of blue and red lines computed at the graphene temperature $T_g = 77$ K and 500 K, respectively. In each pair, the lower line is for a graphene sheet with $\Delta = 0.2$ eV and the upper line is for a graphene sheet with $\Delta = 0.1$ eV.

As is seen in Figure 3, at both temperatures the contribution F_M decreases in magnitude with increasing separation. In the separation region considered, this decrease occurs to the relatively small values at $T_g = 77$ K and to the classical limit (29) at $T_g = 500$ K. In doing so, the sign of F_M remains negative which corresponds to the attractive force.

The role of the contribution F_r is somewhat different. The sign of F_r in (6) is determined by the sign of the quantity Θ in (7) and of the imaginary parts of R_{TM} and R_{TE}

defined in (4). Thus, F_r can be both negative and positive. The quantity Θ is negative for $T_g > T_E$ and is positive for $T_g < T_E$. As to the sign of $\text{Im } R_{\text{TM}}$ and $\text{Im } R_{\text{TE}}$, it depends on the relative contributions of the frequency regions (9) and (10). In the region (9), $\text{Im } R_{\text{TM,TE}}$ is positive and in the region (10) — negative. The computational results for F_r are obtained by Equations (6), (4) and respective expressions for the polarization tensor at real frequencies presented in Section 3.

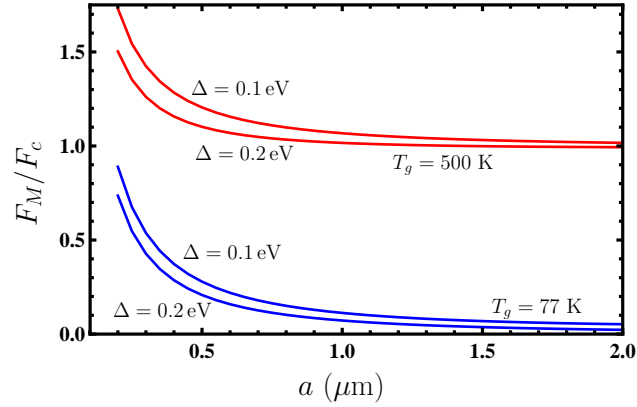


Figure 3. The ratio of the first contribution to the nonequilibrium force acting on a nanoparticle on the source side of cooled to $T_g = 77$ K and heated to $T_g = 500$ K gapped graphene sheets to the classical limit of an equilibrium at $T_E = 300$ K force acting between the same nanoparticle and an ideal metal plane is shown by the pairs of blue and red lines, respectively, as the function of separation. In each pair, the lower line is for a graphene sheet with the mass-gap parameter $\Delta = 0.2$ eV and the upper line is for a graphene sheet with $\Delta = 0.1$ eV.

In Figure 4(a), we plot the ratio F_r/F_c as the function of separation at the graphene temperature $T_g = 77$ K and in Figure 4(b) — for $T_g = 500$ K (the blue and red pairs of lines, respectively). In both cases the lower and upper lines are for the graphene sheets with $\Delta = 0.2$ and 0.1 eV, respectively. From Figure 4(a) one can see that for a graphene sheet with $\Delta = 0.2$ eV at $T_g = 77$ K the contribution F_r remains negligibly small at all separations considered, whereas it increases monotonously with increasing separation for a graphene sheet with $\Delta = 0.1$ eV. The sign of F_r remains negative. Here, the main contribution to F_r given by the frequency region (10) is negative leading to $F_r < 0$.

In Figure 4(b), the sign of F_r is positive for a graphene sheet with $\Delta = 0.2$ eV and changes from the positive to negative for graphene with $\Delta = 0.1$ eV. This means that, at the separations considered, the main contribution to F_r for a graphene sheet with $\Delta = 0.2$ eV given by the frequency region (10) is positive leading to $F_r > 0$. If $\Delta = 0.1$ eV, the relative role of the frequency regions (9) and (10) is different depending on separation. At short distances the dominant region is (10) and $F_r > 0$, whereas at separations exceeding approximately $0.5 \mu\text{m}$ the dominant contribution is given by the region (9) and $F_r < 0$.

By comparing Figure 1 with Figures 3 and 4(a), it is seen that at short separations the major contribution to F_{neq} for a graphene sheet at $T_g = 77$ K is given by F_M for both values of the mass-gap parameter. At large separations, the major contribution to F_{neq} is given by F_r for graphene with $\Delta = 0.1$ eV, whereas the relatively small values of F_{neq} for graphene with $\Delta = 0.2$ eV are determined by F_M .

In a similar way, by comparing Figure 2 with Figures 3 and 4(b), we conclude that at short separations the major contributions to F_{neq} for graphene sheets at $T_g = 500$ K with both values of Δ are also given by F_M . These contributions, however, are slightly decreased by the impact of F_r which is of the opposite sign. At large separations the major contribution to F_{neq} is again given by F_M for both values of Δ , but for $\Delta = 0.1$ eV its magnitude is slightly increased at the expense of F_r .

At the intermediate separation distances, the value of the nonequilibrium dispersion force acting on a nanoparticle on the source side of gapped graphene sheet is determined by the joint action of both contributions F_M and F_r .

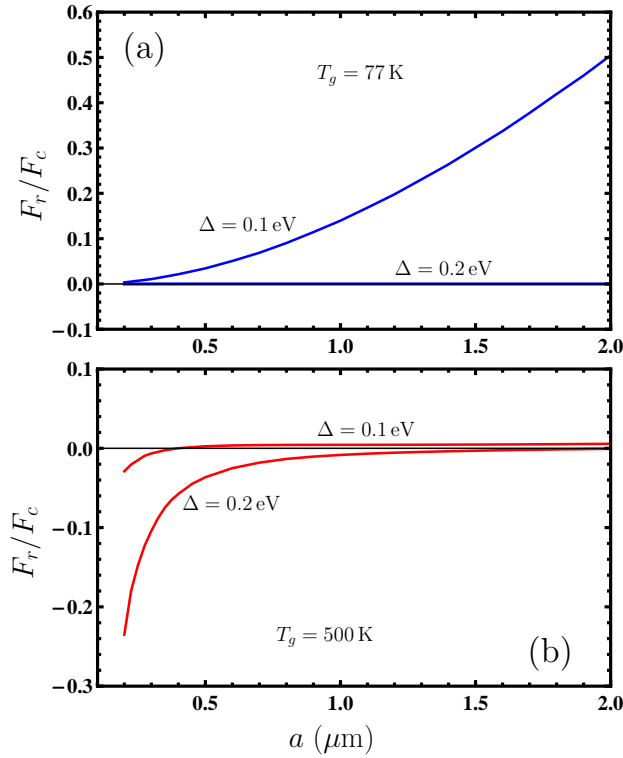


Figure 4. The ratio of the second contribution to the nonequilibrium force acting on a nanoparticle on the source side of (a) cooled to $T_g = 77\text{ K}$ and (b) heated to $T_g = 500\text{ K}$ gapped graphene sheets to the classical limit of an equilibrium at $T_E = 300\text{ K}$ force acting between the same nanoparticle and an ideal metal plane is shown by the pairs of blue and red lines, respectively, as the function of separation. In each pair, the lower line is for a graphene sheet with the mass-gap parameter $\Delta = 0.2\text{ eV}$ and the upper line is for a graphene sheet with $\Delta = 0.1\text{ eV}$.

5. Discussion

In this article, we have investigated the dispersion (Casimir-Polder) force acting on a nanoparticle on the source side of a gapped graphene sheet in the nonequilibrium situations when the graphene temperature is not equal to the nanoparticle temperature coinciding with the temperature of the environment. Both cases when the graphene temperature is lower and higher than that of the environment were considered.

It was shown that the nonzero value of the mass-gap parameter results in new properties of the nonequilibrium dispersion force as compared to the case of thermal equilibrium. Specifically, for a cooled graphene sheet, the variation of the mass-gap parameter makes a lesser and greater impact on the nonequilibrium force than on the equilibrium one at short and large separations, respectively. For a heated graphene sheet, the variation of the mass-gap parameter results in a lesser impact on the nonequilibrium force than on the equilibrium one at all separations considered from 200 nm to $2\text{ }\mu\text{m}$. As opposed to the case of a pristine graphene, for a gapped graphene sheet, the nonequilibrium dispersion force preserves an attractive character at all separations considered.

We emphasize that the above results were obtained using the dielectric response of graphene expressed via the polarization tensor. The latter quantity was found in the framework of the Dirac model on the solid foundation of quantum field theory with no recourse to any phenomenological methods. Thus, in the application region

of the Dirac model discussed in Section 3, these results possess a highest degree of reliability. In fact graphene and other 2D materials, such as silicene, stanene, germanene etc. [90–95], are unique in that some of their properties can be investigated basing on the most fundamental physical principles. The nonequilibrium dispersion force acting on nanoparticles on the source side of gapped graphene considered above presents one more example of this kind.

6. Conclusions

To conclude, the above results give the possibility to control the nonequilibrium dispersion interaction between nanoparticles and a graphene sheet by varying the mass-gap parameter of this sheet and its temperature. The need for such a control is apparent when taken into account that both nanoparticles of different kinds and graphene are already widely used in various micro- and nanodevices, including the field-effect transistors, integrated nanoparticle-biomolecule systems, electrochemical sensors and biosensors etc. [6,7,18,19,39–46]. The theoretical methods used in the design of these micro- and nanodevices are often based on the phenomenology and computer simulation, rather than on the fundamental physical principles. It is hoped that an employment of the methods of fundamental physics will further accelerate the progress in this rapidly developing field of applied science.

In the future, it would be interesting to extend the obtained results to graphene sheets deposited on substrates made of metallic and dielectric materials and to consider the case of doped graphene characterized by some nonzero chemical potential. This will provide further possibilities to control the nonequilibrium dispersion interaction in micro- and nanodevices incorporating nanoparticles and graphene sheets for their functionality.

Funding: The work of O.Yu.T., was supported by the Russian Science Foundation under Grant No. 21-72-20029. G.L.K. was partially funded by the Ministry of Science and Higher Education of Russian Federation ("The World-Class Research Center: Advanced Digital Technologies," contract No. 075-15-2022-311 dated April 20, 2022). The research of V.M.M. was partially carried out in accordance with the Strategic Academic Leadership Program "Priority 2030" of the Kazan Federal University.

References

1. Kyslychyn, D.; Piatnytsia, V.; Lozovski, V. Electrodynamic interaction between a nanoparticle and the surface of a solid. *Phys. Rev. E* **2013**, *88*, 052403.
2. Ma, C.; Huangfu, X.; He, Q.; Ma, J.; Huang, R. Deposition of engineered nanoparticles (ENPs) on surfaces in aquatic systems: a review of interaction forces, experimental approaches, and influencing factors. *Environ. Sci. Poll. Res.* **2018**, *25*, 33056–33081.
3. Summueang, C.; Boonchui, S. Electrical interaction between nanoparticle and surface of material. *IOP Conf. Ser.: Mater. Sci. Eng.* **2019**, *526*, 012016.
4. Wang, H.; Zhang, W.; Zeng, S.; Shen, C.; Jin, C.; Huang, Y. Interactions between nanoparticles and fractal surfaces. *Water Res.* **2019**, *151*, 296–309.
5. Andrén, D.; Länk, N.O.; Šípová-Jungová, H.; Jones, S.; Johansson, P.; Käll, M. Surface Interactions of Gold Nanoparticles Optically Trapped against an Interface. *J. Phys. Chem. C* **2019**, *123*, 16406–16414.
6. Luo, X.; Morrin, A.; Killard, A.J.; Smyth, M.R. Application of Nanoparticles in Electrochemical Sensors and Biosensors. *Electroanal.* **2006**, *18*, 319–326.
7. Willner, I.; Baron, R.; Willner, B. Integrated nanoparticle-biomolecule systems for biosensing and bioelectronics. *Biosens. Bioelectron.* **2007**, *22*, 1841–1852.
8. Lynch, I.; Dawson, K.A. Protein-nanoparticle interactions. *Nanotoday* **2008**, *3*, 40–47.
9. Verma, A.; Stellacci, F. Effect of Surface Properties on Nanoparticle-Cell Interactions. *Nano. Micro. Small* **2010**, *6*, 12–21.
10. Saptarshi, S.R.; Duschl, A.; Lopata, A.L. Interaction of nanoparticles with proteins: relation to bio-reactivity of the nanoparticle. *J. Nanobiotech.* **2013**, *11*, 26.
11. Dyubo, D.; Tsybin, O.Yu. Particles-on-surface sensor with potential barriers embedded in a semiconductor target. *J. Phys.: Conf. Ser.* **2019**, *1326*, 012003.
12. Perera, Y.R.; Hill, R.A.; Fitzkee, N.C. Protein Interactions with Nanoparticle Surfaces: Highlighting Solution NMR Techniques. *Isr. J. Chem.* **2019**, *59*, 962–979.

13. Park S.J. Protein-Nanoparticle Interaction: Corona Formation and Conformational Changes in Proteins on Nanoparticles. *Int. J. Nanomed.* **2020**, *15*, 5783–5802.
14. Dyubo, D.; Tsybin, O.Yu. Computer Simulation of a Surface Charge Nanobiosensor with Internal Signal Integration. *Biosensors* **2021**, *11*, 397.
15. González-García, L.E.; MacGregor, M.N.; Visalakshan, R.M.; Lazarian, A.; Cavallaro, A.A.; Morsbach, S.; Mierczynska-Vasilev, A.; Mailänder, V.; Landfester, K.; Vasilev, K. Nanoparticles Surface Chemistry Influence on Protein Corona Composition and Inflammatory Responses. *Nanomater.* **2022**, *12*, 682.
16. de Macedo, E.F.; Santos, N.S.; Nascimento, L.S.; Mathey, R.; Brenet, S.; de Moura, M.S.; Hou, Y.; Tada, D.B. Interaction between Nanoparticles, Membranes and Proteins: A Surface Plasmon Resonance Study. *Int. J. Mol. Sci.* **2023**, *24*, 591.
17. Vilquin, A.; Bertin, V.; Raphaël, E.; Dean, D.S.; Saler, T.; McGraw, J.D. Nanoparticle Taylor Dispersion Near Charged Surfaces with Open Boundary. *Phys. Rev. Lett.* **2023**, *130*, 038201.
18. Sun, W. Interaction forces between a spherical nanoparticle and a flat surface. *Phys. Chem. Chem. Phys.* **2014**, *16*, 5846–5854.
19. Moreno, F.; García-Cámara, B.; Saiz, J.M.; González, F. Interaction of nanoparticles with substrates: effects on the dipolar behaviour of the particles. *Opt. Express* **2008**, *16*, 12487–12504.
20. Castro Neto, A.H.; Guinea, F.; Peres, N.M.R.; Novoselov, K.S.; Geim, A.K. The electronic properties of graphene. *Rev. Mod. Phys.* **2009**, *81*, 109–162.
21. Aoki, H.; Dresselhaus, M.S. (Eds.) *Physics of Graphene*; Springer: Cham, Switzerland, 2014.
22. Katsnelson, M.I. *The Physics of Graphene*; Cambridge University Press: Cambridge, UK, 2020.
23. Judd, T.E.; Scott, R.G.; Martin, A.M.; Kaczmarek, B.; Fromhold, T.M. Quantum reflection of ultracold atoms from thin films, graphene and semiconductor heterostructures. *New J. Phys.* **2011**, *13*, 083020.
24. Chaichian, M.; Klimchitskaya, G.L.; Mostepanenko, V.M.; Tureanu, A. Thermal Casimir-Polder interaction of different atoms with graphene. *Phys. Rev. A* **2012**, *86*, 012515.
25. Arora, B.; Kaur, H.; Sahoo, B.K. C_3 coefficients for the alkali atoms interacting with a graphene and carbon nanotube. *J. Phys. B* **2014**, *47*, 155002.
26. Kaur, K.; Kaur, J.; Arora, B.; Sahoo, B.K. Emending thermal dispersion interaction of Li, Na, K and Rb alkali-metal atoms with graphene in the Dirac model. *Phys. Rev. B* **2014**, *90*, 245405.
27. Klimchitskaya, G.L.; Mostepanenko, V.M. Impact of graphene coating on the atom-plate interaction. *Phys. Rev. A* **2014**, *89*, 062508.
28. Cysne, T.; Kort-Kamp, W.J.M.; Oliver, D.; Pinheiro, F.A.; Rosa, F.S.S.; Farina, C. Tuning the Casimir-Polder interaction via magneto-optical effects in graphene. *Phys. Rev. A* **2014**, *90*, 052511.
29. Kaur, K.; Arora, B.; Sahoo, B.K. Dispersion coefficients for the interactions of the alkali-metal and alkaline-earth-metal ions and inert-gas atoms with a graphene layer. *Phys. Rev. A* **2015**, *92*, 032704.
30. Henkel, C.; Klimchitskaya, G.L.; Mostepanenko, V.M. Influence of the chemical potential on the Casimir-Polder interaction between an atom and gapped graphene or a graphene-coated substrate. *Phys. Rev. A* **2018**, *97*, 032504.
31. Khusnutdinov, N.; Kashapov, R.; Woods, L.M. Casimir-Polder effect for a stack of conductive planes. *Phys. Rev. A* **2016**, *94*, 012513.
32. Khusnutdinov, N.; Kashapov, R.; Woods, L.M. Thermal Casimir and Casimir-Polder interactions in N parallel 2D Dirac materials. *2D Mater.* **2018**, *5*, 035032.
33. Klimchitskaya G.L.; Mostepanenko V.M. Nernst heat theorem for an atom interacting with graphene: Dirac model with nonzero energy gap and chemical potential. *Phys. Rev. D* **2020**, *101*, 116003.
34. Khusnutdinov, N.; Emelianova, N. The Low-Temperature Expansion of the Casimir-Polder Free Energy of an Atom with Graphene. *Universe* **2021**, *7*, 70.
35. Klimchitskaya, G.L. The Casimir-Polder interaction of an atom and real graphene sheet: Verification of the Nernst heat theorem. *Mod. Phys. Lett. A* **2020**, *35*, 2040004.
36. Klimchitskaya, G.L.; Mostepanenko, V.M. Casimir and Casimir-Polder Forces in Graphene Systems: Quantum Field Theoretical Description and Thermodynamics. *Universe* **2020**, *6*, 150.
37. Das, B.; Choudhury, B.; Gomathi, A.; Manna, A.K.; Pati, S.K.; Rao, C.N.R. Interaction of Inorganic Nanoparticles with Graphene. *ChemPhysChem* **2011**, *12*, 937–943.
38. Biehs, S.-A.; Agarwal, G.S. Anisotropy enhancement of the Casimir-Polder force between a nanoparticle and graphene. *Phys. Rev. A* **2015**, *90*, 042510; Erratum in **2015**, *91*, 039901.
39. Devi, J.M. Simulation Studies on the Interaction of Graphene and Gold Nanoparticle. *Int. J. Nanosci.* **2018**, *17*, 1760043.
40. Low, S.; Shon, Y.-S. Molecular interactions between pre-formed metal nanoparticles and graphene families. *Adv. Nano Res.* **2018**, *6*, 357–375.
41. Huang, L.-W.; Jeng, H.-T.; Sua, W.-B.; Chang, C.-S. Indirect interactions of metal nanoparticles through graphene. *Carbon* **2021**, *174*, 132.
42. Williams, G.; Kamat, P.V. Graphene-Semiconductor Nanocomposites: Excited-State Interactions between ZnO Nanoparticles and Graphene Oxide. *Langmuir* **2009**, *25*, 13869–13873.
43. Donnelly, M.; Mao, D.; Park, J.; Xu, G. Graphene field-effect transistors: the road to bioelectronics. *J. Phys. D: Appl. Phys.* **2018**, *51*, 493001.

44. Puigpelat, E.; Ignés-Mullol, J.; Sagués, F.; Reigada, R. Interaction of Graphene Nanoparticles and Lipid Membranes Displaying Different Liquid Orderings: A Molecular Dynamics Study. *Langmuir* **2019**, *35*, 16661–16668.
45. Liu, H.; Hao, C.; Zhang, Y.; Yang, H.; Sun, R. The interaction of graphene oxide-silver nanoparticles with trypsin: Insights from adsorption behaviors, conformational structure and enzymatic activity investigations. *Coll. Surf. B: Biointerf.* **2021**, *202*, 111688.
46. Klimchitskaya, G.L.; Mostepanenko, V.M.; Velichko, E.N. Casimir pressure in peptide films on metallic substrates: Change of sign via graphene coating. *Phys. Rev. B* **2021**, *103*, 245421.
47. Lifshitz, E.M. The theory of molecular attractive forces between solids. *Zh. Eksp. Teor. Fiz.* **1955**, *29*, 94–110; Translated: *Sov. Phys. JETP* **1956**, *2*, 73–83.
48. Dzyaloshinskii, I.E.; Lifshitz, E.M.; Pitaevskii, L.P. The general theory of van der Waals forces. *Usp. Fiz. Nauk* **1961**, *73*, 381–422; Translated: *Adv. Phys.* **1961**, *10*, 165–209.
49. Lifshitz, E.M.; Pitaevskii, L.P. *Statistical Physics, Part II*; Pergamon: Oxford, UK, 1980.
50. Bordag, M.; Fialkovsky, I.V.; Gitman, D.M.; Vassilevich, D.V. Casimir interaction between a perfect conductor and graphene described by the Dirac model. *Phys. Rev. B* **2009**, *80*, 245406.
51. Fialkovsky, I.V.; Marachevsky, V.N.; Vassilevich, D.V. Finite-temperature Casimir effect for graphene. *Phys. Rev. B* **2011**, *84*, 035446.
52. Bordag, M.; Klimchitskaya, G.L.; Mostepanenko, V.M.; Petrov, V.M. Quantum field theoretical description for the reflectivity of graphene. *Phys. Rev. D* **2015**, *91*, 045037; Erratum in **2016**, *93*, 089907.
53. Bordag, M.; Fialkovskiy, I.; Vassilevich, D. Enhanced Casimir effect for doped graphene. *Phys. Rev. B* **2016**, *93*, 075414; Erratum in **2017**, *95*, 119905.
54. Henkel, C.; Joulain, K.; Mulet, J.P.; Greffet, J.J. Radiation forces on small particles in thermal near fields. *J. Opt. A: Pure Appl. Opt.* **2002**, *4*, S109–114.
55. Antezza, M.; Pitaevskii, L.P.; Stringari, S. New Asymptotic Behavior of the Surface-Atom Force out of Thermal Equilibrium. *Phys. Rev. Lett.* **2005**, *95*, 113202.
56. Antezza, M.; Pitaevskii, L.P.; Stringari, S.; Svetovoy, V.B. Casimir-Lifshitz force out of thermal equilibrium. *Phys. Rev. A* **2008**, *77*, 022901.
57. Bimonte, G. Scattering approach to Casimir forces and radiative heat transfer for nanostructured surfaces out of thermal equilibrium. *Phys. Rev. A* **2009**, *80*, 042102.
58. Messina, R.; Antezza, M. Scattering-matrix approach to Casimir-Lifshitz force and heat transfer out of thermal equilibrium between arbitrary bodies. *Phys. Rev. A* **2011**, *84*, 042102.
59. Krüger, M.; Bimonte, G.; Emig, T.; Kardar, M. Trace formulas for nonequilibrium Casimir interactions, heat radiation, and heat transfer for arbitrary bodies. *Phys. Rev. B* **2012**, *86*, 115423.
60. Bimonte, G.; Emig, T.; Krüger, M.; Kardar, M. Dilution and resonance-enhanced repulsion in nonequilibrium fluctuation forces. *Phys. Rev. A* **2011**, *84*, 042503.
61. Krüger, M.; Emig, T.; Bimonte, G.; Kardar, M. Non-equilibrium Casimir forces: Spheres and sphere-plate. *Europhys. Lett.* **2011**, *95*, 21002.
62. Klimchitskaya, G.L.; Mostepanenko, V.M.; Sedmik, R.I.P. Casimir pressure between metallic plates out of thermal equilibrium: Proposed test for the relaxation properties of free electrons. *Phys. Rev. A* **2019**, *100*, 022511.
63. Klimchitskaya, G.L.; Mostepanenko, V.M. Casimir-Polder Interaction of an Atom with a Cavity Wall Made of Phase-Change Material out of Thermal Equilibrium. *Atoms* **2020**, *9*, 4.
64. Ingold, G.-L.; Klimchitskaya, G.L.; Mostepanenko, V.M. Nonequilibrium effects in the Casimir force between two similar metallic plates kept at different temperatures. *Phys. Rev. A* **2020**, *101*, 032506.
65. Khandekar, C.; Buddhiraju, S.; Wilkinson, P.R.; Gimzewski, J.K.; Rodriguez, A.W.; Chase, C.; Fan, S. Nonequilibrium lateral force and torque by thermally excited nonreciprocal surface electromagnetic waves. *Phys. Rev. B* **2021**, *104*, 245433.
66. Castillo-López, S.G.; Esquivel-Sirvent, R.; Pirruccio, G.; Villarreal, C. Casimir forces out of thermal equilibrium near a superconducting transition. *Sci. Rep.* **2022**, *12*, 2905.
67. Klimchitskaya, G.L.; Mostepanenko, V.M.; Tsybin, O.Yu. Casimir-Polder attraction and repulsion between nanoparticles and graphene in out-of-thermal-equilibrium conditions. *Phys. Rev. B* **2022**, *105*, 195430.
68. Gusynin, V.P.; Sharapov, S.G.; Carbotte, J.P. On the universal ac optical background in graphene. *New J. Phys.* **2009**, *11*, 095013.
69. Pyatkovsky, P.K. Dynamical polarization, screening, and plasmons in gapped graphene. *J. Phys. Condens. Matter* **2009**, *21*, 025506.
70. Klimchitskaya, G.L.; Mohideen, U.; Mostepanenko, V.M. The Casimir force between real materials: Experiment and theory. *Rev. Mod. Phys.* **2009**, *81*, 1827–1885.
71. Bordag, M.; Klimchitskaya, G.L.; Mohideen, U.; Mostepanenko, V.M. *Advances in the Casimir Effect*; Oxford University Press: Oxford, UK, 2015.
72. Klimchitskaya, G.L.; Mostepanenko, V.M.; Sernelius, B.E. Two approaches for describing the Casimir interaction with graphene: density-density correlation function versus polarization tensor. *Phys. Rev. B* **2014**, *89*, 125407.
73. Klimchitskaya, G.L.; Korikov, C.C.; Petrov, V.M. Theory of reflectivity properties of graphene-coated material plates. *Phys. Rev. B* **2015**, *92*, 125419; Erratum in **2016**, *93*, 159906.

-
74. Klimchitskaya, G.L.; Mostepanenko, V.M. Reflectivity properties of graphene with nonzero mass-gap parameter. *Phys. Rev. A* **2016**, *93*, 052106.
 75. Klimchitskaya, G.L.; Mostepanenko, V.M. Optical properties of dielectric plates coated with gapped graphene. *Phys. Rev. B* **2017**, *95*, 035425.
 76. Klimchitskaya, G.L.; Mostepanenko, V.M. Maximum reflectance and transmittance of films coated with gapped graphene in the context of the Dirac model. *Phys. Rev. A* **2018**, *97*, 063817.
 77. Klimchitskaya, G.L.; Mostepanenko, V.M. Conductivity of pure graphene: Theoretical approach using the polarization tensor. *Phys. Rev. B* **2016**, *93*, 245419.
 78. Klimchitskaya, G.L.; Mostepanenko, V.M. Quantum electrodynamic approach to the conductivity of gapped graphene. *Phys. Rev. B* **2016**, *94*, 195405.
 79. Klimchitskaya, G.L.; Mostepanenko, V.M.; Petrov, V.M. Conductivity of graphene in the framework of Dirac model: Interplay between nonzero mass gap and chemical potential. *Phys. Rev. B* **2017**, *96*, 235432.
 80. Klimchitskaya, G.L.; Mostepanenko, V.M. Kramers-Kronig relations and causality conditions for graphene in the framework of Dirac model. *Phys. Rev. D* **2018**, *97*, 085001.
 81. Zhu, T.; Antezza, M.; Wang, J.-S. Dynamical polarizability of graphene with spatial dispersion. *Phys. Rev. B* **2021**, *103*, 125421.
 82. Liu, M.; Zhang, Y.; Klimchitskaya, G.L.; Mostepanenko, V.M.; Mohideen, U. Demonstration of Unusual Thermal Effect in the Casimir Force from Graphene. *Phys. Rev. Lett.* **2021**, *126*, 206802.
 83. Liu, M.; Zhang, Y.; Klimchitskaya, G.L.; Mostepanenko, V.M.; Mohideen, U. Experimental and theoretical investigation of the thermal effect in the Casimir interaction from graphene. *Phys. Rev. B* **2021**, *104*, 085436.
 84. Bordag, M.; Pirozhenko, I.G. Surface plasmon on graphene at finite T . *Int. J. Mod. Phys. B* **2016**, *30*, 1650120.
 85. Obrecht, J.M.; Wild, R.J.; Antezza, M.; Pitaevskii, L.P.; Stringari, S.; Cornell, E.A. Measurement of the temperature dependence of the Casimir-Polder force. *Phys. Rev. Lett.* **2007**, *98*, 063201.
 86. Galassi, M.; Davies, J.; Theiler, J.; Gough, B.; Gungman, G.; Alken, P.; Booth, M.; Rossi, F.; Ulerich, R. GNU Scientific Library Reference Manual, 2021. Available online: <https://www.gnu.org/software/gsl/doc/latex/gsl-ref.pdf> (accessed on 8 May 2023).
 87. Boost C++ Libraries. Available online: <https://www.boost.org> (accessed on 8 May 2023).
 88. Boost Multiprecision Library. Available online: <https://github.com/boostorg/multiprecision> (accessed on 8 May 2023).
 89. OpenMP Application Programming Interface. Available online: <https://www.openmp.org/specifications> (accessed on 8 May 2023).
 90. Cahangirov, S.; Topsakal, M.; Aktürk, E.; Sahin, H.; Ciraci, S. Two- and One-Dimensional Honeycomb Structures of Silicon and Germanium. *Phys. Rev. Lett.* **2009**, *102*, 236804.
 91. Xu, M.; Liang, T.; Shi, M.; Chen, H. Graphene-Like Two-Dimensional Materials. *Chem. Rev.* **2013**, *113*, 5, 3766–3798.
 92. Yuhara, J.; Fujii, Y.; Nishino, K.; Isobe, N.; Nakatake, M.; Xian, L.; Rubio, A.; and Le Lay, G. Large area planar stanene epitaxially grown on Ag(1 1 1). *2D Mater.* **2018**, *5*, 025002.
 93. Mu, X.; Yu, W.; Yuan, J.; Lin, S.; Zhang, G. Interface and surface engineering of black phosphorus: a review for optoelectronic and photonic applications. *Mater. Futures* **2022**, *1*, 012301.
 94. Xu, R.; Guo, J.; Mi, S.; Wen, H.; Pang, F.; Ji, W.; Cheng, Z. Advanced atomic force microscopies and their applications in two-dimensional materials: a review. *Mater. Futures* **2022**, *1*, 032302.
 95. Yan, Z.; Yang, H.; Yang, Z.; Ji, C.; Zhang, G.; Tu, Y.; Du, G.; Cai, S.; Lin, S. Emerging Two-Dimensional Tellurene and Tellurides for Broadband Photodetectors. *Small* **2022**, *18*, 2200016.